Photoionization of helium nanodroplets doped with rare gas atoms

Jeong Hyun Kim, Darcy S. Peterka, Chia C. Wang, and Daniel M. Neumark[a)]
Department of Chemistry, University of California, Berkeley, California 94720 and Chemical Sciences Division, Lawrence Berkeley National Laboratory, Berkeley, California 94720

(Received 9 March 2006; accepted 12 April 2006; published online 1 June 2006)

Photoionization of He droplets doped with rare gas atoms (Rg=Ne, Ar, Kr, and Xe) was studied by time-of-flight mass spectrometry, utilizing synchrotron radiation from the Advanced Light Source from 10 to 30 eV. High resolution mass spectra were obtained at selected photon energies, and photoion yield curves were measured for several ion masses (or ranges of ion masses) over a wide range of photon energies. Only indirect ionization of the dopant rare gas atoms was observed, either by excitation or charge transfer from the surrounding He atoms. Significant dopant ionization from excitation transfer was seen at 21.6 eV, the maximum of He $2p\ ^1$P absorption band for He droplets, and from charge transfer above 23 eV, the threshold for ionization of pure He droplets. No Ne^+ or Ar^+ signal from droplet photoionization was observed, but peaks from He_nNe^+ and He_nAr^+ were seen that clearly originated from droplets. For droplets doped with Rg=Kr or Xe, both Rg^+ and He_nRg^+ ions were observed. For all rare gases, Rg_2^+ and $He_nRg_m^+$ $(n,m \geqslant 1)$ were produced by droplet photoionization. Mechanisms of dopant ionization and subsequent dynamics are discussed. © *2006 American Institute of Physics*. [DOI: 10.1063/1.2202313]

I. INTRODUCTION

Liquid He nanodroplets, comprising more than 10^3 atoms, provide a unique environment for studying molecules and clusters.[1–4] Though He atoms in droplets should be more inert than any other solvents, they interact with dopants in a collective fashion.[5] Most research on doped helium droplets has focused on the rotational, vibrational, and electronic spectroscopy of dopant-in-droplet systems, which usually results in spectral shifts compared to the isolated species.[6,7] However, there is growing interest in both photoionization and electron impact ionization experiments on doped helium droplets.[8–11] Those studies have been focused on ion formation mechanisms in droplets, the interaction of dopant ions with the droplet environment, and post-ionization dynamics. Rare gas (Rg) atoms such as Ne, Ar, Kr, and Xe should be among the most weakly interacting dopants, and should also show readily discernible size-dependent trends. These considerations have motivated several studies on the ionization of rare gas doped droplets using electron impact ionization.[12–15] In this work, we report a complementary study using photoionization, rather than electron impact, on droplets doped with rare gas atoms, making use of widely tunable vacuum ultraviolet (VUV) photons to probe the energy dependence of ionization dynamics within droplets.

In pure He droplets, the high photon energies required for electronic excitation and photoionization necessitate using VUV light from synchrotrons. Joppien *et al.*[16] observed VUV fluorescence emission from He droplets excited from 20 to 25 eV. The fluorescence excitation spectrum of large He droplets showed a broad absorption band centered at 21.6 eV that is clearly correlated to the atomic He $1s-2p$ transition at 21.2 eV, and weaker features between 23 and 24.6 eV, the ionization energy (IE) of atomic He. Photoionization studies of pure droplets by Fröchtenicht *et al.*[8] showed that the threshold for ionization was around 23 eV, well below IE(He); this difference was attributed to the formation of He_2^+ or larger cation clusters within the droplet. Photoelectron imaging experiments in our group showed that excitation between 23 and 24.6 eV resulted in extremely slow photoelectrons,[17] with an average energy <1 meV, suggesting an indirect ionization mechanism and considerable final state interaction between the photoelectron and droplet atoms; more recent work above IE(He) indicates a very different mechanism dominated by direct ionization.[18]

In doped droplets, direct ionization of the dopant by single or multiphoton absorption is possible, as is ionization resulting from photoexcitation of the surrounding He atoms. Fröchtenicht *et al.*[8] found that the latter mechanism dominated in the single photon ionization of droplets doped with SF_6. In that work, the SF_5^+ signal from doped droplets roughly mirrored the He droplet absorption spectrum measured by Joppien *et al.*[16] implying that dopant ionization occurred by either excitation transfer (i.e., Penning ionization) or charge transfer from the surrounding He atoms, depending on whether the photon energy was below or above the pure droplet ionization threshold of 23 eV. On the other hand, laser-based, multiphoton ionization experiments on droplets doped with metal clusters[19] or aromatic molecules[11,20] showed direct ionization of the dopant species.

Droplets doped with rare gases (Ne, Ar, Kr, and Xe) have been studied previously with electron impact ionization. Lewerenz *et al.*[12] performed a detailed early study of rare gas pickup in He droplets, obtaining cross sections for capture of both single and multiple rare gas atoms; the latter process resulted in the formation of a rare gas "subcluster" within the droplet. A key conclusion from this paper was that

a)Author to whom correspondence should be addressed. Electronic mail: dneumark@berkeley.edu

the ion signals for Kr_k^+ $(k=1-4)$ ions at different scattering chamber pressures could be fit to the Poisson distribution for pickup of rare gas atoms, implying that the fragmentation of dopant cluster ions after ionization was negligible and the mass distribution of ions reflected the distribution of neutral aggregates in droplets.

In related work, Janda and co-workers[13–15] and Halberstadt and co-workers[21–23] carried out a series of experimental and theoretical studies on electron impact ionization of He droplets doped with Ne, Ar, and Xe. They found that the ionic products from droplets doped with one or more rare gas atoms depended strongly on the identity of the rare gas and droplet size. For example, clusters doped with single Ar or Ne atoms produced only He_nRg^+ ions, while Ar_2^+ and Ne_2^+ were the dominant fragments from droplets with two or more rare gas atoms,[13,14] showing considerably more fragmentation than the results reported for Kr-doped clusters.[12] Clusters doped with single Xe atoms produced bare Xe^+ ions,[15] in contrast to the results for Ne and Ar. The mechanism of dopant ionization was considered at length in these studies and attributed to charge transfer from He^+ produced by electron impact within the droplet. Since this process competes with formation of He_2^+, the probability of charge transfer with the dopant was, in general, found to be significantly less than unity.

To gain further insight into the ionization mechanism of dopants in He droplets, we performed high resolution time-of-flight mass spectrometry of He droplets doped with Ne, Ar, Kr, and Xe using synchrotron radiation of the Advanced Light Source, varying the photon energy from 10 to 30 eV. Product mass distributions below and above the threshold for ionization in droplets were determined, and the high resolution of the mass spectrometer yielded a more accurate identification of products than was possible in the previous electron impact studies. The photoion yield (PIY) as a function of photon energy provided a sensitive diagnostic as to whether ions at a particular mass were produced by droplet photoionization or from ionization of background gas. No unambiguous Ne^+ or Ar^+ signal from droplet photoionization was seen, although there was considerable Kr^+ and Xe^+ signal from droplets. We observed Rg_2^+ and $He_nRg_m^+$ $(m \geqslant 1)$ from droplet ionization for all rare gas dopants. In particular, we found that droplets doped with two Kr or Xe atoms yield significant $He_nRg_2^+$ signal. The PIY curves are interpreted in terms of dopant ionization via both excitation transfer and charge transfer from the surrounding He atoms and compared to previous electron impact studies.

II. EXPERIMENT

The experiments were carried out on the Chemical Dynamics Beamline at the Advanced Light Source. Our experimental apparatus has been described in detail elsewhere.[17] A continuous He droplet beam was produced by expanding 60 bars of helium gas through a 5 μm aperture of a source at cryogenic temperature (16–18 K), making droplets with ~8000 He atoms on average. The droplet beam then passed through a 1.5 mm skimmer and entered the pickup region where a 2 in. long pickup cell with 2.5 mm apertures is located. The rare gases were introduced to the pickup cell through a gas line with a variable leak valve. The pressure in the pickup cell was monitored by a microion gauge and kept at about 1×10^{-5} torr. Under these conditions, one can calculate the Poisson distribution indicating the probability that n rare gas atoms will be picked up by a He droplet, using the capture cross sections determined by Lewerenz *et al.*;[12] the calculated distributions for Ar, Kr, and Xe are shown in Fig. 1. The plot demonstrates that most of our pickup signal originated from droplets with one or two dopant atoms.

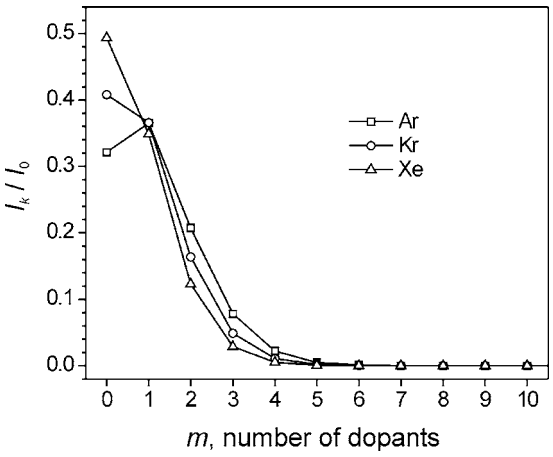

FIG. 1. Calculated Poisson distributions I_k/I_0 for pickup of k rare gas atoms under conditions of our experiment (average droplet size $\langle N\rangle \sim 8000$ and pickup cell pressure of 1×10^{-5} torr). Capture cross sections for Ar, Kr, and Xe were scaled from the values reported in Ref. 12.

After passing through another 2 mm skimmer, doped He droplets were ionized by tunable synchrotron radiation (10–30 eV), which crossed the droplet beam perpendicularly in the main chamber. The resulting photoions were then accelerated into the Wiley-McLaren-type time-of-flight mass spectrometer (0.6 m) and detected with microchannel plates of 40 mm diameter. The ion counts were recorded using a multichannel scalar (Fast Comtec, P7886) at 1 ns time resolution. The pseudocontinuous synchrotron radiation was chopped by an optical chopper rotating at ~600 Hz.[24] The combination of the chopped synchrotron beam and the high voltage extraction pulse triggered by the beam yielded time-of-flight mass spectra with a resolution of $m/\Delta m \sim 350$ at a repetition rate of ~20 kHz. Therefore, data acquisition times were as short as a few minutes for a typical time-of-flight mass spectrum with millions of sweeps; these rapid acquisition times were crucial given the limited amount of synchrotron beam time available to us.

III. RESULTS

Figure 2 shows the mass spectrum of pure He clusters at 24.75 eV, just above the ionization energy of atomic He, 24.6 eV. The intensity of He^+ (4 amu) is far higher than other masses and is clipped in the current viewgraph for clarity. The local maximum at 56 amu (He_{14}^+) is a well known magic number in both photoionization and electron impact ionization of pure He droplets.[8,25,26] As seen in the inset of Fig. 2, the noise level of the mass spectrum is extremely low, typically less than ten counts for 2×10^6

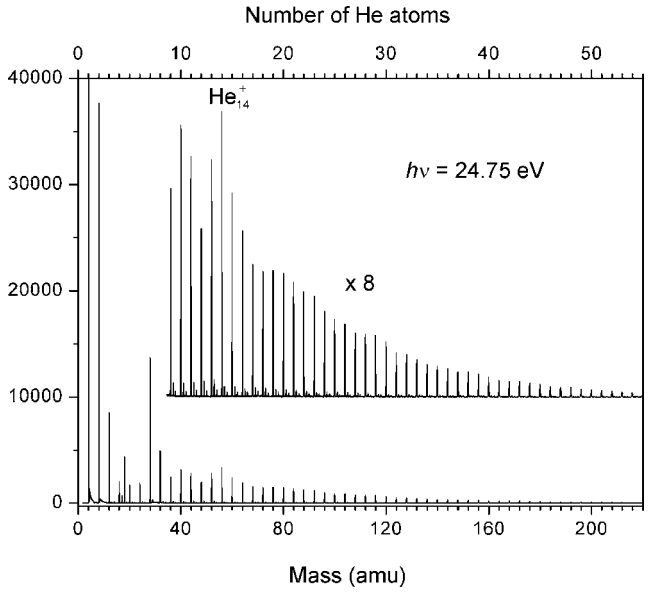

FIG. 2. Time-of-flight mass spectrum of pure He droplets at $h\nu$=24.75 eV, above IE(He), dominated by He_n^+ peaks. The intensity of the He^+ peak was more than 250 000 counts and thus clipped in the current graph to make other masses more viewable. Inset shows magic number at n=14.

sweeps, compared to 2.5×10^5 counts for He^+. As the photon energy is varied from 21.0 to 25.5 eV, He_2^+ and larger cluster ions begin to appear at about 23 eV, consistent with previous photoionization and photoelectron studies of pure droplets.[8,17] The major background ions such as H_2O^+, N_2^+, and O_2^+ are mainly from the residual gas in the detection chamber, showing no correlation with He droplet beam.

Figure 3 shows the photoionization mass spectra of pure and rare gas doped He droplets at 21.6 eV, corresponding to the center of the $2p$ ^{1}P excitation band.[16] This energy is sufficient to ionize rare gases other than He. The mass spectrum in Fig. 3(a) for pure droplets at this energy shows contributions from background signals (i.e., H_2O^+, N_2^+, and O_2^+) but, as expected, no evidence of the extended He_n^+ peaks from droplet ionization. There are, however, some He^+ and He_2^+ ions in the mass spectrum. They are either from the second order diffraction from the grating or from the energetic secondary electrons generated by the strong fluorescence emission. Figures 3(b)–3(e) display the mass spectra of He droplets doped with each of rare gases, i.e., Ne, Ar, Kr, and Xe, respectively. In contrast to Fig. 3(a), these spectra show a series of peaks spaced every 4 amu, attributed to $He_nRg_m^+$ ions (Rg=Ne, Ar, Kr, and Xe). This signal must originate from doped droplets. For Ne and Ar doped droplets, the smallest, easily observable species of this type are He_4Ne^+ (36 amu) and He_9Ar^+ (76 amu). We note that even smaller He_nNe^+ and He_nAr^+ clusters are more difficult to observe because of the intense background peaks at the same masses from, for example, N_2, O_2, and CO_2.

Because Kr and Xe have several natural isotopes, all of the mass peaks after Kr^+ and Xe^+ are 1 or 2 amu apart, resulting in a congested mass spectrum. Nevertheless, the closely spaced peaks are resolved owing to the high resolution of our time-of-flight mass spectrometer. In Figs. 3(d) and 3(e), there are long progressions of He_nKr^+ and He_nXe^+

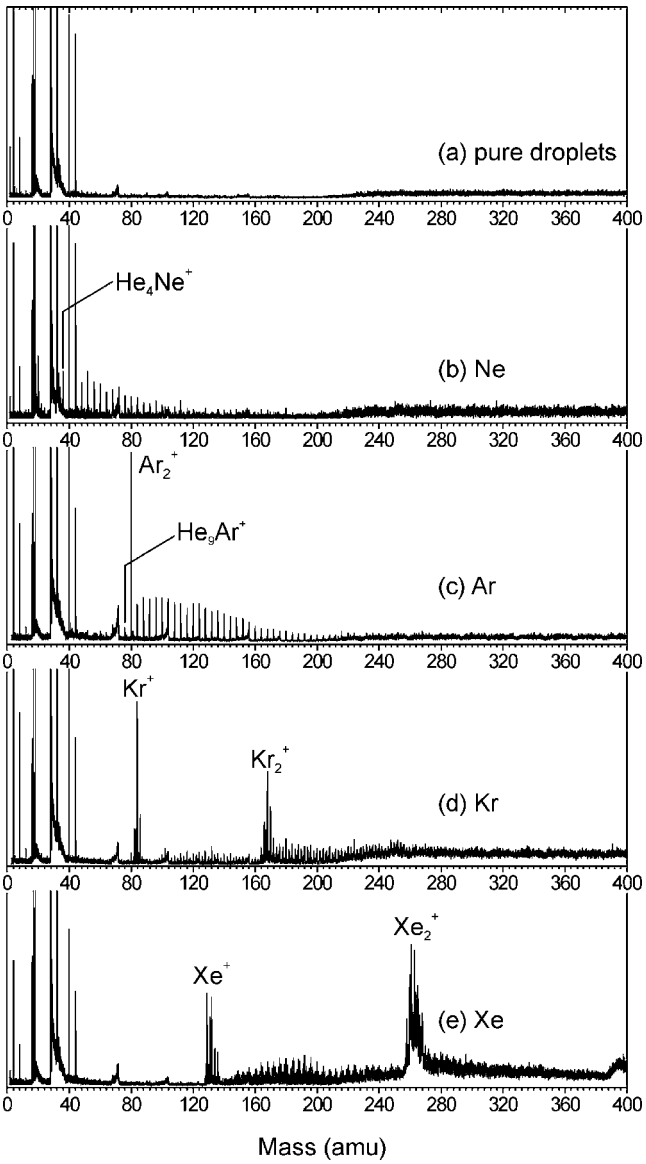

FIG. 3. Time-of-flight mass spectra of (a) pure and doped He droplets with (b) Ne, (c) Ar, (d) Kr, and (e) Xe at $h\nu$=21.6 eV, the maximum of the He $2p$ absorption in pure droplets. The progressions of small peaks separated by 4 amu are from $He_nRg_m^+$.

peaks extending up to the lightest isotopes of Kr_2^+ and Xe_2^+, which correspond to n=18 and 30, respectively. Beyond these peaks, it is difficult to tell from Fig. 3 whether the peaks correspond to He_nRg^+ or $He_nRg_2^+$ ions. This question is clarified in Fig. 4, which shows an expanded view of the mass spectra starting around the Kr^+ and Xe^+ features. As pointed out previously, there is no contribution from pure He_n^+ peaks in the mass spectra at 21.6 eV, so the mass distribution of $He_nKr_m^+$ and $He_nXe_m^+$ is seen directly, without any further correction. In Fig. 4(a), between the Kr^+ and Kr_2^+ features, peaks at $4n$ amu from $He_n{}^{84}Kr^+$ ions are twice as large as peaks at $(4n+2)$ amu from $He_n{}^{82}Kr^+$ and $He_n{}^{86}Kr^+$, while the peak intensities above Kr_2^+ alternate in intensity every amu (see insets, Fig. 4). For Xe, the intensity modulations are also more pronounced below the Xe_2^+ peaks. Both trends in the experimental mass spectra are reproduced in simulations of the isotope patterns (also shown in Fig. 4)

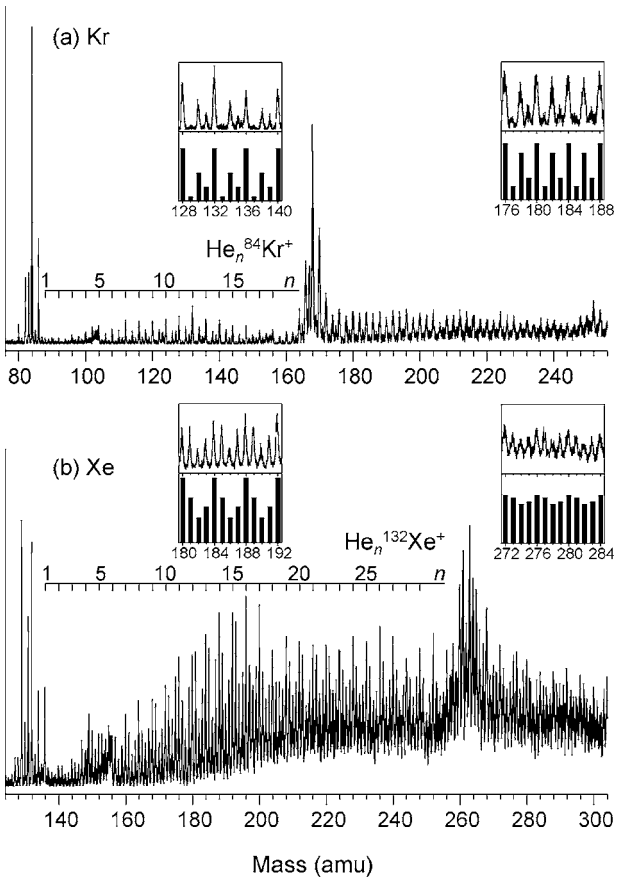

FIG. 4. Expanded view of time-of-flight mass spectra of (a) Kr and (b) Xe doped droplets at $h\nu$=21.6 eV. Combs indicate positions of $He_n{}^{84}Kr^+$ and $He_n{}^{132}Xe^+$ for given ranges of n. Insets show the experimental and simulated isotope patterns for He_nKr^+, $He_nKr_2^+$, He_nXe^+, and $He_nXe_2^+$.

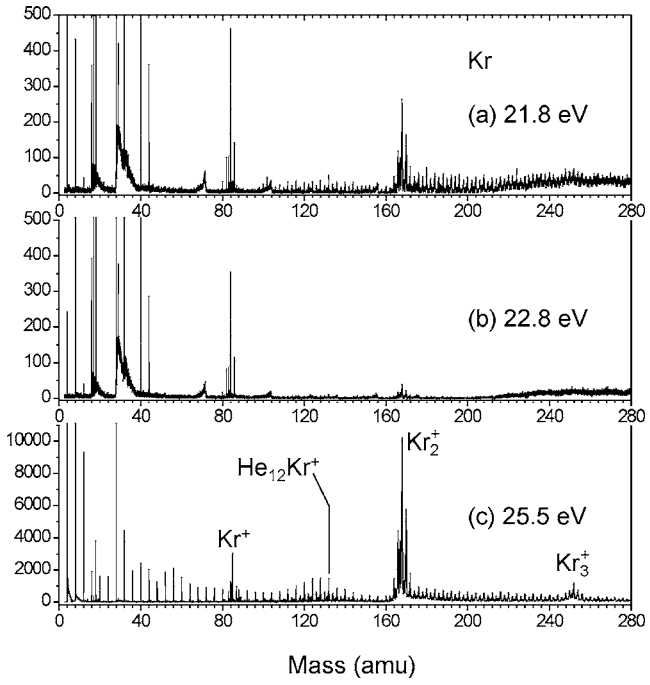

FIG. 5. Time-of-flight mass spectra of Kr doped droplets at (a) 21.8 eV, near the maximum of He 2p absorption; (b) 22.8 eV, where virtually no absorption of He droplets occurs; (c) 25.5 eV, above the IE of atomic He. Note that the ion counts in (c) are much higher than in (a) and (b).

assuming one Rg atom below the Rg_2^+ peak and two above the peak, indicating that the peaks after Kr_2^+ and Xe_2^+ are mainly from $He_nKr_2^+$ and $He_nXe_2^+$, rather He_nKr^+ and He_nXe^+ ions with higher n.

Figure 5 shows the mass spectra of He droplets doped with Kr at three photon energies: 21.8, 22.8, and 25.5 eV. The second energy lies in a region where there is very little pure droplet absorption,[16] while the third is well above IE(He). The spectrum in Fig. 5(a) is essentially the same as that in Fig. 3(d), with significant contributions from He_nKr^+ along with bare and clustered Kr_2^+. These features are nearly gone at 22.8 eV [Fig. 4(b)], with only the Kr^+ feature remaining. Since the droplet absorption at this energy is very weak, this feature is mostly attributed to background Kr gas that effuses from the pickup cell and is ionized in the detection chamber.

At 25.5 eV [Fig. 5(c)], the overall signal is enhanced considerably, as indicated by the y axes in Fig. 5. There is significant signal from He_n^+ ions, similar to that seen in Fig. 2, that is absent at 21.8 eV [Fig. 5(a)]. These ions can be formed by ionization of pure *and* doped droplets, because the efficiency of charge transfer to the dopant is less than unity.[13] The He_n^+ progression is seen up to the highest masses shown in Fig. 5. Between the Kr^+ and Kr_2^+ peaks, two interleaved progressions spaced by 4 amu are seen. In the more intense progression, each peak has contributions from He_n^+, (the largest contribution) $He_n{}^{80}Kr^+$, and $He_n{}^{84}Kr^+$. Each peak in the weaker progression is from multiple He atoms complexed to ^{82}Kr and ^{86}Kr. The profile of the cluster distribution for He_nKr^+ at 25.5 eV is obviously not monotonic and shows a maximum at n=12; this is less noticeable in Fig. 5(a). Beyond Kr_2^+, there are again two progressions: a more intense series of peaks from He_n^+ and $He_nKr_2^+$ isotopomers for which the Kr_2^+ total mass is divisible by 4, and a weaker progression from $He_nKr_2^+$ isotopomers such as $^{82}Kr^{84}Kr^+$. At even higher masses, a small cluster of peaks from Kr_3^+ is seen.

The ratio of Kr^+ to Kr_2^+ varies with photon energy, even though the pickup cell pressure was kept constant in all spectra shown in Fig. 5. While the Kr^+ intensity at 25.5 eV is only five times larger than at 21.8 eV, for instance, the peak at 168 amu ($^{84}Kr_2^+$) has increased by a factor of 40. However, direct comparison between monomer and dimer ion intensities can be misleading because at the lower photon energy, a larger fraction of the Kr^+ signal originates from ionization of Kr atoms effusing out of the pickup cell.

When the Kr pressure in the pickup cell is raised to 7×10^{-5} torr, the Kr_2^+ and Kr_3^+ peaks become more intense than Kr^+ (see Fig. 6). In addition, we observe mass peaks that are grouped at around 216 and 300 amu (marked as A and B), which correspond to $He_{12}Kr_2^+$ and $He_{12}Kr_3^+$, respectively. Features A and B are distinguished from the progression of peaks from He_n^+ that passes through the Kr_2^+ and Kr_3^+ features in that they have the natural isotope abundance patterns of Kr_2 and Kr_3. If we look at the spectrum more closely, there is a group of peaks around 132 amu, which also look similar to the abundance distribution of Kr isotopes. However, the $He_{12}Kr_2^+$ and $He_{12}Kr_3^+$ peaks are far more noticeable than $He_{12}Kr^+$.

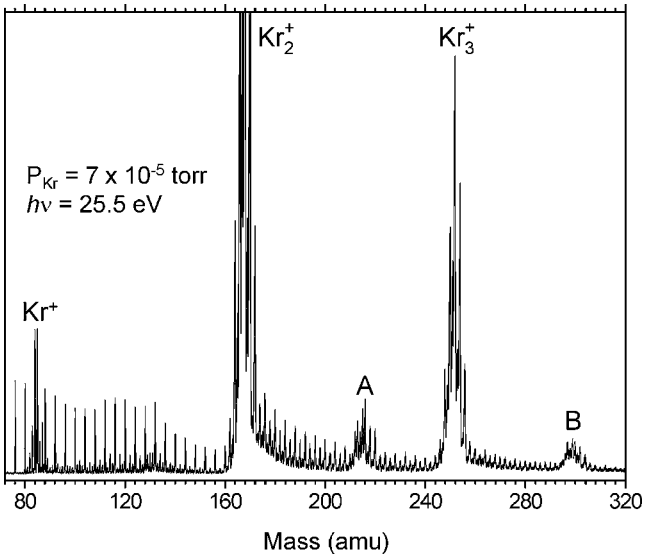

FIG. 6. Time-of-flight mass spectrum of Kr doped droplets at high pickup pressure, 7×10^{-5} torr, and $h\nu$=25.5 eV. The peaks following Kr^+ are from both pure He clusters and He_nKr^+. The grouped peaks marked as A (at ~216 amu) and B (at ~300 amu) have the isotope distribution of Kr_2^+ and Kr_3^+, respectively. Therefore, these features correspond to magic-numbered clusters of $He_{12}Kr_2^+$ and $He_{12}Kr_3^+$ (see text).

Figures 7–9 show the photoion yield as a function of energy for various masses, obtained by integrating the indicated mass peaks as the photon energy is varied. PIY's for monomer rare gas ions are shown in Fig. 7. Ne, Kr, and Xe have at least three isotopes and the mass is specified at the upper left corner of each panel. Because He_n^+ peaks will occur every 4 amu above 23 eV, we chose to monitor masses that do not overlap with these peaks whenever possible (which can be done for everything but Ar). The gray bar indicates the $2p$ absorption of He droplets (21.6 eV). All the ions in Fig. 7 show an abrupt rise at the atomic IEs, an indication (see below) that much of the photoion signal comes from bare atoms effusing from the gas cell rather than from atoms entrained in droplets. In the case of Ne, the IE

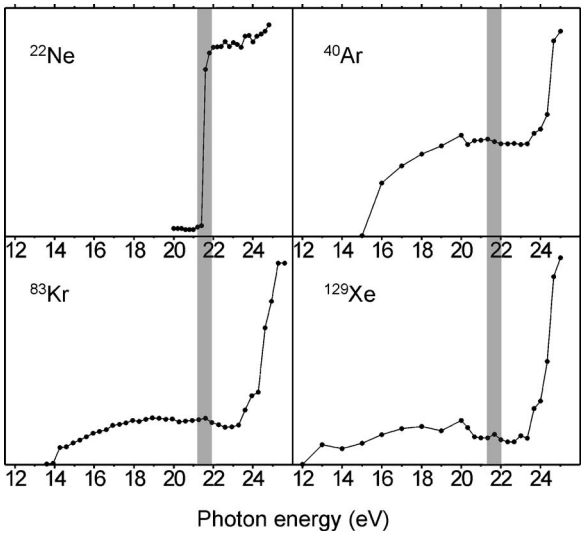

FIG. 7. Photoion yields for monomer ions of Ne, Ar, Kr, and Xe. The mass of the detected isotope is shown at the upper left corner of each panel. The gray bars indicate the location of He $2p$ absorption of droplets.

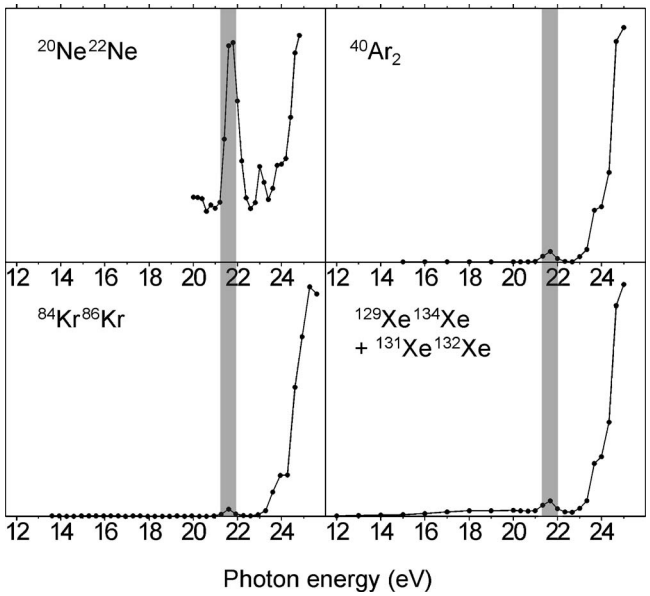

FIG. 8. Photoion yields for dimer ions of Ne, Ar, Kr, and Xe. For Ne, Kr, and Xe, isotopic combinations were chosen that do not have the same masses as pure He_n^+ cluster ions.

(21.56 eV) coincides with the absorption maximum in He droplets. The PIY for Ar^+ is flat above the IE until 23 eV, the ionization threshold for He droplets, above which it rises sharply. As discussed below, this rise is likely from He_{10}^+ at the same mass. The isotopes chosen for Kr^+ and Xe^+ do not overlap any He_n^+ peaks. Their PIY's show a small peak at 21.6 eV and rise sharply above 23 eV.

In contrast to the monomer ions, PIY's for rare gas dimer ions (Fig. 8) have negligible background ion counts below 21 eV. Each shows a clear feature around 21.6 eV, and increased signal above 23 eV. In all rare gas dimers except $^{20}Ne^{22}Ne^+$, the steep rise above 23 eV is much more prominent than the feature at 21.6 eV. Larger cluster ions such as Ar_3^+ and Ar_4^+ have PIY's similar to that seen for Ar_2^+; these data are not shown here. Finally, in Fig. 9, we show PIY's for masses that could correspond to He_nRg^+ (but also to pure He_n^+ ions in some cases). Since members of a He_nRg^+ series for each rare gas showed a similar dependence on photon energy, the PIY's for several peaks in each series were added together in Fig. 9. For Kr and Xe, we chose to look at masses that fall between pure He_n^+ peaks and could therefore obtain background-free PIY's. Again, all the PIY's in Fig. 9 show a distinct peak at 21.6 eV. Except for Ne, PIY's of each He_nRg^+ series are similar to those of Rg_2^+.

IV. DISCUSSION

In this section, we first consider the origin of the photoionization signals and the mechanism by which ionization occurs. The photoionization results are then compared to the more extensive experimental and theoretical work on electron impact ionization of droplets doped with rare gas atoms. This comparison provides a context for interpreting many of our results in more detail in Sec. IV C.

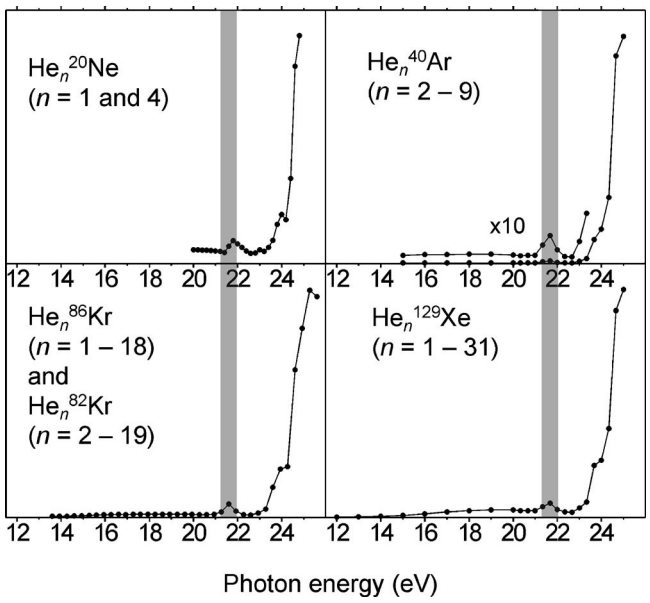

FIG. 9. Photoion yields of He_nRg^+ (Rg=Ne, Ar, Kr, and Xe) for masses lying between Rg^+ and Rg_2^+. The values of n were selected in such a manner that the corresponding peaks do not overlap with either pure He clusters or major background gas peaks whenever possible.

A. Origin and mechanism of photoionization signals

In discussing the various mass spectral features in Figs. 3–6, it is important to be able to distinguish between ions produced by photoionization of doped droplets versus atoms effusing from the gas cell. This distinction is clear in the case of Rg_m^+ ($m \geq 2$, $Rg \neq He$) or He_nRg^+ cluster ions, which must originate from doped droplets, but it is an issue for Rg^+ monomer ion signal. The PIY curves in Figs. 7–9 provide an excellent means of distinguishing between the two cases, and also provide considerable insight into the ionization mechanism.

As pointed out in Sec. I, photoionization of a dopant within a He droplet can occur by a direct or indirect mechanism, with the latter involving excitation or ionization of the surrounding He atoms. The two mechanisms can be distinguished by the PIY curve for a particular ion product; the indirect mechanism is dominant if this curve approximately tracks the absorption spectrum of the pure droplet, as was seen for the SF_5^+ product from ionization of droplets doped with SF_6.[8] For example, the $^{84}Kr^{86}Kr^+$ PIY curve in Fig. 8 shows a small peak at 21.6 eV, corresponding to the $2p$ excitation in pure droplets,[16] an increase in signal starting at 23 eV, the onset for ionization of droplets,[8,17] and a much larger increase starting at 24.6 eV, corresponding to IE(He). Hence, it is clear that this ion is produced by indirect processes: a Penning-type ionization process from excitation transfer at 21.6 eV, charge transfer processes above 24.6 eV, and, possibly, both processes between 23 and 24.6 eV (see Sec. IV C). Given that the parent Kr_m subcluster is surrounded by ~8000 He atoms, the dominance of indirect processes in single photon ionization is not surprising. We note that the relative intensities of the PIY curve in the three spectral regions are a convolution of the absorption cross section and the dopant ionization probability, as discussed further in Sec. IV C.

The Ar_2^+ and Xe_2^+ PIY curves in Fig. 8 and the four He_nRg^+ curves in Fig. 9 all show essentially the same spectral pattern as the Kr_2^+ curve, indicating that the same ionization mechanisms are prevalent. The Ne_2^+ PIY curve shows enhanced intensity around 21.6 eV, illustrating that excitation transfer is particularly efficient for droplets doped with at least two Ne atoms; this point is discussed in Sec. IV C. In the He_nAr^+ curve in Fig. 9, however, the feature at 21.6 eV is about a factor of 10 lower intensity relative to the signal above 23 eV compared to He_nKr^+ and He_nXe^+. This discrepancy results from He_nAr^+ having the same mass as pure He cluster ions, which can be formed by ionization of pure and doped droplets above 23 eV. Note that although the masses of the $^{40}Ar_2^+$, $He_n{}^{20}Ne^+$, and $He_n{}^{40}Ar^+$ ions coincide with those of pure He_n^+ ions, pure droplets will not ionize at 21.6 eV. That is, if those mass peaks were solely from pure helium clusters, the feature at 21.6 eV should be missing in PIY curves.

The PIY curves in Fig. 7 for the Rg^+ ions are very different from those in Figs. 8 and 9. The curves for Ne^+ and Ar^+ begin at the IEs of the two atoms and show no enhancement at 21.6 eV. The signal levels for Ne^+ and Ar^+ below 23 eV are essentially the same regardless of whether the droplet beam is present so this ion signal is, in fact, from rare gas atoms effusing from the gas cell, and is not associated with He droplets. The rise in the $^{40}Ar^+$ signal above 23 eV occurs only when the droplet beam is on but is almost certainly due to He_{10}^+ (at the same mass) from ionization of pure (and doped) He droplets. The PIY curves for $^{83}Kr^+$ and $^{129}Xe^+$ show signal as low as the atomic IEs from effusive background gas, but they also exhibit small peaks at 21.6 eV and a steep rise above 23 eV that cannot be from pure He clusters. Hence, it appears that some of bare monomer ions are produced by indirect ionization of He droplets doped with Kr and Xe. However, the intensity of He_nXe^+, when summed over n=1–31, is about ten times higher than Xe^+ at 21.6 eV, so that Rg^+ production is clearly a minor channel even for droplets doped with Xe.

Thus far, we have not addressed the issue of subcluster parentage and the extent to which fragmentation of a rare gas subcluster within a droplet occurs upon photoionization. The calculated Poisson distributions for rare gas pickup (see Fig. 1) are quite useful in this regard. For example, under the operating conditions in Figs. 3 and 4, there are many more clusters with two dopant atoms than three. It is therefore likely that the Rg_2^+ ions for all rare gases and the $He_nRg_2^+$ products identified for Rg=Kr and Xe originate from droplets with two dopant atoms. The parentage of Rg^+ (for Kr and Xe) and He_nRg^+ ions for all the rare gases is less straightforward to determine directly from our data. Previous electron impact ionization experiments,[13–15] described in more detail in the following section, indicate that He_nRg^+ comes primarily from singly doped droplets, whereas bare Kr^+ and Xe^+ can originate from either singly or doubly doped droplets.

B. Photoionization versus electron impact ionization

Most previous studies on the ionization of doped droplets utilized electron impact ionization.[9,12–15] Collisions of

droplets with energetic electrons (~60 eV) induce extensive fragmentation. The dopant ionization mechanism is thought to be production of He^+ by electron impact, followed by migration of this charge through the droplet until the dopant (with much lower IE in all cases) is ionized. Charge migration competes with charge localization to form He_2^+, at which point the droplet fragments to form He_n^+ products owing to the energy released upon formation of He_2^+.[25] Simulations by Callicoatt *et al.*[13] indicate that unless dopant ionization occurs within three hops, on average, corresponding to 60–80 fs, He_2^+ will form and the dopant will not be ionized. If charge transfer to the dopant occurs, then depending on the nature and number of dopant species, one observes either bare dopant ions or the dopant ions clustered to multiple He atoms.

Lewerenz *et al.*[12] reported the mass spectra of He droplets doped with Kr and obtained the pressure dependence of Kr_k^+ ion signal for $k \geqslant 1$. For each value of k, the pressure dependence of the Kr_k^+ signal could be fit to Poisson distribution. Hence, the Kr_k^+ distribution was considered as reflecting the neutral Kr_k abundance, so that fragmentation of the subcluster upon ionization was largely suppressed by the surrounding He atoms.

The papers by Janda and co-workers[13–15] have yielded a more complex picture of ionization and fragmentation of doped He clusters. They measured the yield of Rg_m^+ and $He_nRg_m^+$ products as a function of pickup cell pressure and obtained a global fit to their results in simulations where the charge transfer probability and fragmentation of the rare gas subcluster were treated as parameters. This analysis showed that ionization of droplets singly doped with Ne or Ar did not produce bare Rg^+ ions but rather a progression of He_nRg^+ fragments, while droplets doped with two Ne or Ar atoms primarily yielded Rg_2^+ as the main dopant ionization channel. Droplets doped with Xe led to both Xe^+ and He_nXe^+, while droplets doped with two Xe atoms formed Xe^+, Xe_2^+, and He_nXe^+ in varying proportions depending on the droplet size.

Some of these trends could be explained quite intuitively. For example, in droplets doped with two Ar atoms, ionization of Ar_2 by charge transfer leads to highly vibrationally excited Ar_2^+, and subsequent vibrational cooling leads to evaporation of all (or most) of the He atoms leaving bare Ar_2^+ as the main product.[13] The formation of He_nRg^+ ions from droplets doped with one Ne or Ar was attributed to a radiative charge transfer transition from a $RgHe^+$ state to a $HeRg^+$ state, with the emitted photon removing much of the energy associated with this otherwise exothermic charge transfer process.[13,14] In the case of droplets doped with single Xe atoms,[15] charge transfer from $XeHe^+$ to an excited, repulsive $HeXe^+$ state was proposed, leading to ejection of electronically excited Xe^+ from the droplet.

Many of the trends seen in the electron impact studies were reproduced in our photoionization mass spectra, not only at photon energies above the onset for pure droplet ionization but also at 21.6 eV, where dopant ionization can occur only via excitation transfer. For example, as pointed out in the previous section, we did not observe any Ne^+ or Ar^+ from droplet photoionization, while we saw He_nNe^+ and He_nAr^+ fragments that, by analogy with the electron impact experiments, most likely originate from singly doped droplets. We also saw bare Kr^+ and Xe^+ along with progressions in which these ions are complexed to multiple He atoms. Finally, we observed bare Rg_2^+ peaks from all the doped droplets.

Our experiment does, however, clearly show that there is significant $He_nRg_2^+$ production from droplets doped with Kr and Xe, at both 21.6 and 25.5 eV (see Fig. 4). As mentioned in the previous section, this signal most likely arises from droplets doped with two rare gas atoms. In the electron impact studies,[12,15] the mass resolution was not sufficient to determine whether products beyond Kr_2^+ or Xe_2^+ contained one or two Rg atoms, although it was claimed that very few $He_nXe_2^+$ fragments were produced by electron impact.[15]

In the case of droplets doped with Ar, one cannot tell if the progression of peaks spaced by 4 amu starting from Ar_2^+ [Fig. 3(c)] is based on one or two Ar atoms. In the work of Callicoatt *et al.*,[13] the experimental mass spectra for smaller He clusters ($\langle N \rangle = 1000-3000$) also showed a long progression of peaks spaced by 4 amu; this progression starts well below the Ar_2^+ peak but continues beyond it. On the basis of their simulations, this entire progression was assigned to He_nAr^+ ions for the smaller clusters, and even for clusters as large as ours, at most 5% of this progression was assigned to $He_nAr_2^+$. However, subsequent electron impact work on droplets doped with Ne did show significant $He_nNe_2^+$ production from droplets as small as $\langle N \rangle = 2800$ doped with one ^{20}Ne and one ^{22}Ne atom.[14] This observation, when combined with our results for Kr and Xe, suggests that there may be more $He_nAr_2^+$ than indicated in the original analysis.

We note that all the Rg_2^+ ions are bound by 1.0–1.3 eV (Ref. 27) and that photoionization of neutral Rg_2, like electron impact ionization, should produce the dimer cation with vibrational excitation corresponding to a significant fraction of this well depth. However, even complete vibrational relaxation from the top of the Rg_2^+ well should not evaporate all the He atoms in droplets comprising a few thousand atoms or more, given that the binding energy of each He is 0.6 meV in a neutral droplet, and the average is presumably considerably higher in a droplet with a charged dopant. Hence, the observation of Rg_2^+ ions complexed to multiple He atoms appears consistent with the known energetics of the species involved, particularly for the large droplets studied in our experiment. Moreover, recent experiments by Lewis *et al.*[28] indicate that the translational energy of He atoms leaving a droplet containing a vibrationally excited, ionic chromophore exceeds what would be expected from thermal evaporation. If such a mechanism were operative here, it would be even likelier that complete relaxation of vibrationally excited Rg_2^+ would not lead to loss of all the surrounding He atoms.

Finally, the mass spectrum obtained for Kr doped droplets at high pickup pressure in Fig. 6 presents another point of comparison with electron impact ionization studies, in this case the work by Lewerenz *et al.*[12] Our spectra show clear evidence for enhanced $He_{12}Kr_2^+$ and $He_{12}Kr_3^+$ production at 25.5 eV, implying that these ionic clusters are particularly stable. The mass spectrum by Lewerenz *et al.*, obtained under similar conditions, shows maxima at approximately the same masses as these species, although it is difficult to make

an unambiguous correspondence owing to the lower mass resolution in that work. Nonetheless it appears that regardless of whether ionization occurs via photons or electrons, these ionic products are particularly prominent. Since they are prominent only at high pickup pressures we expect that they result from fragmentation of larger neutral Kr subclusters.

C. Mechanism and dynamics of doped-droplet photoionization

The discussion in Sec. IV A showed that photoionization of droplets doped with rare gas atoms results in dopant ionization via either excitation transfer or charge transfer from the surrounding He atoms, depending on the photon energy. Above 24.6 eV, the ionization energy of atomic He, we expect the dopant ionization mechanism to be similar to that induced by electron impact ionization and described in Sec. IV B, i.e., formation of He^+ within the droplet followed by charge hopping and, ultimately, charge transfer to the dopant. Excitation at 21.6 eV presumably results in a droplet excited state comprising an excited He atom in its $2p\ ^1P$ Rydberg state interacting with its neighboring He atoms, although the exact nature of this excited state remains an open question.[29] This excitation can also migrate toward the dopant and ionize it.

As pointed out in Sec. IV B, charge transfer to the dopant occurs with less than unit efficiency because it competes with localization to form He_2^+, which is subsequently ejected from the droplet. Similar considerations are expected to hold for excitation transfer. The interaction between a Rydberg atom (or molecule) with its diffuse electron cloud and the other He atoms in the droplet is repulsive and results in expulsion of this species from the droplet. In fact, the electronic absorption spectrum of pure droplets is obtained by monitoring fluorescence from ejected He^* and He_2^* as a function of excitation energy.[16,30–32]

We can gain a qualitative understanding of the relative efficiencies of charge versus excitation transfer to rare gas dopants from the PIY curves in Figs. 7 and 8. In all cases except Ne_2^+, the feature at 21.6 eV is considerably weaker than the signal above the pure droplet ionization threshold, 23 eV, and weaker still than the signal above IE(He). In contrast, the 21.6 eV peak dominates the fluorescence excitation spectrum of pure droplets.[16] Hence, all indications are that ionization of rare gas dopant by excitation transfer is less efficient than by charge transfer. Theoretical studies of the relative rates of excitation transfer versus Rydberg ejection would be of considerable interest in light of our results.

In Fig. 8, the $^{20}Ne^{22}Ne^+$ PIY curve differs from the other Rg_2^+ curves in that the peak at 21.6 eV is enhanced considerably compared to the signal at higher energy. This effect may arise from the near agreement of IE (Ne) and He $2p$ absorption because many of autoionizing states of Ne are located at around 21.6 eV. Excitation transfer from the He $2p$ state would become very effective when the donor (He^*) is able to transfer the energy to the acceptor (Ne_2) in resonance. Interestingly, Fig. 8 shows another distinct band at $\sim$23 eV in Ne_2^+, which coincides with the location of the He $3p$ state. Again, the proximity of Ne states and He excitation might explain the enhancement of the excitation transfer features. This should be also true for $He_n{}^{20}Ne^+$, but the feature at 21.6 eV is overwhelmed by the rise at 23 eV due to pure helium clusters at the same masses.

Dopant ionization via excitation transfer will be highly exothermic in all cases except Ne. The energy released by this process will be partitioned between the internal (nuclear and electronic) degrees of freedom of the ionic cluster and the ejected photoelectron. Hence, measurement of the photoelectron spectrum resulting from droplet excitation at 21.6 eV will indicate how much energy remains in the ionic cluster. This information should prove very useful in understanding the cluster fragmentation patterns seen in our mass spectra.

Thus far, we have not discussed the mechanism by which dopant ionization occurs between 23 and 24.6 eV. In this range, photoionization of pure droplets occurs through an indirect mechanism that is as yet not fully understood.[8,24] The proposed mechanism involves formation of highly excited He_2^* which then autoionizes to He_2^+ or a larger cationic subcluster, producing an exceedingly slow (<1 meV) photoelectron. Ionization competes with ejection of He^* and/or He_2^* and is believed to be a minor channel. In doped droplets, ionization of the rare gas dopant can thus occur either by excitation transfer from He^* or He_2^* before either species is ejected from the cluster, or by charge transfer from the He_n^+ cationic subcluster. It is not straightforward to distinguish between these two mechanisms based on the data presented here. Again, measurement of the photoelectron spectrum of droplets doped with rare gas atoms and excited in this intermediate energy range would provide a valuable diagnostic. The observation of very slow electrons, like those seen for the pure droplets,[17] would suggest that ionization of the He medium occurs before dopant ionization, supporting the charge transfer mechanism, whereas higher energy photoelectrons would presumably be a signature of dopant ionization via a highly exothermic Penning-type mechanism.

V. CONCLUSIONS

In this paper, the photoionization of He droplets doped with Ne, Ar, Kr, and Xe was investigated using synchrotron radiation from 10 to 30 eV. Time-of-flight mass spectra were obtained at selected photon energies, and photoion yield (PIY) curves were measured for various ion masses as a function of photon energy. Our results showed that dopant ionization occurs via an indirect mechanism involving either excitation transfer or charge transfer from the surrounding He atoms. Excitation transfer occurs when the droplets are excited around 21.6 eV, corresponding to the droplet analog of the $1s-2p$ transition in atomic He, by charge transfer above 24.6 eV, the ionization energy of He, and possibly by both mechanisms between 23 and 24.6 eV. Comparison of the PIY curves with the absorption spectrum of pure droplets implies that dopant ionization by excitation transfer is less efficient than by charge transfer with the exception of droplets doped with Ne, where there may be resonant enhancement of the excitation transfer process.

No bare Ne^+ or Ar^+ was observed from droplets doped with Ne or Ar; photoionization of these droplets produced only $He_nRg_m^+$ and Rg_m^+ ions, while bare Kr^+ and Xe^+ (and the larger mixed and pure clusters) were produced by photoionization of droplets doped with Kr or Xe. Photoionization of droplets doped with Kr at high pickup cell pressures resulted in enhanced signal for $He_{12}Kr_2^+$ and $He_{12}Kr_3^+$. Many of the trends seen in electron impact ionization of rare gas-doped clusters are seen in photoionization, but the high mass resolution of the work reported here allows for a more definitive identification of the product ions in several cases.

ACKNOWLEDGMENTS

This work was supported by the Director, Office of Science, Office of Basic Energy Science, Chemical Science Division of the U.S. Department of Energy under Contract No. DE-AC02-05CH11231. One of the authors (J.H.K.) gratefully acknowledges Korea Science and Engineering Foundation (KOSEF) for the postdoctoral fellowship.

[1] M. Hartmann, R. E. Miller, J. P. Toennies, and A. Vilesov, Phys. Rev. Lett. **75**, 1566 (1995).
[2] K. Nauta, D. T. Moore, and R. E. Miller, Faraday Discuss. **113**, 261 (1999).
[3] C. Callegari, K. K. Lehmann, R. Schmied, and G. Scoles, J. Chem. Phys. **115**, 10090 (2001).
[4] F. Stienkemeier and A. F. Vilesov, J. Chem. Phys. **115**, 10119 (2001).
[5] M. Hartmann, F. Mielke, J. P. Toennies, A. F. Vilesov, and G. Benedek, Phys. Rev. Lett. **76**, 4560 (1996).
[6] J. P. Toennies and A. F. Vilesov, Annu. Rev. Phys. Chem. **49**, 1 (1998).
[7] J. P. Toennies and A. F. Vilesov, Angew. Chem., Int. Ed. **43**, 2622 (2004).
[8] R. Frochtenicht, U. Henne, J. P. Toennies, A. Ding, M. FieberErdmann, and T. Drewello, J. Chem. Phys. **104**, 2548 (1996).
[9] A. Scheidemann, B. Schilling, and J. P. Toennies, J. Phys. Chem. **97**, 2128 (1993).
[10] B. E. Callicoatt, D. D. Mar, V. A. Apkarian, and K. C. Janda, J. Chem. Phys. **105**, 7872 (1996).
[11] E. Loginov, D. Rossi, and M. Drabbels, Phys. Rev. Lett. **95**, 163401 (2005).
[12] M. Lewerenz, B. Schilling, and J. P. Toennies, J. Chem. Phys. **102**, 8191 (1995).
[13] B. E. Callicoatt, K. Forde, T. Ruchti, L. L. Jung, K. C. Janda, and N. Halberstadt, J. Chem. Phys. **108**, 9371 (1998).
[14] T. Ruchti, K. Forde, B. E. Callicoatt, H. Ludwigs, and K. C. Janda, J. Chem. Phys. **109**, 10679 (1998).
[15] T. Ruchti, B. E. Callicoatt, and K. C. Janda, Phys. Chem. Chem. Phys. **2**, 4075 (2000).
[16] M. Joppien, R. Karnbach, and T. Moller, Phys. Rev. Lett. **71**, 2654 (1993).
[17] D. S. Peterka, A. Lindinger, L. Poisson, M. Ahmed, and D. M. Neumark, Phys. Rev. Lett. **91**, 043401 (2003).
[18] D. S. Peterka, J. H. Kim, C. C. Wang, and D. M. Neumark (unpublished).
[19] P. Radcliffe, A. Przystawik, T. Diederich, T. Doppner, J. Tiggesbaumker, and K. H. Meiwes-Broer, Phys. Rev. Lett. **92**, 173403 (2004).
[20] A. Boatwright, N. A. Besley, S. Curtis, R. R. Wright, and A. J. Stace, J. Chem. Phys. **123**, 021102 (2005).
[21] D. Bonhommeau, A. Viel, and N. Halberstadt, J. Chem. Phys. **120**, 11359 (2004).
[22] C. A. Brindle, M. R. Prado, K. C. Janda, N. Halberstadt, and M. Lewerenz, J. Chem. Phys. **123**, 064312 (2005).
[23] D. Bonhommeau, N. Halberstadt, and A. Viel, J. Chem. Phys. **124**, 024328 (2006).
[24] D. S. Peterka, J. H. Kim, C. C. Wang, and D. M. Neumark, J. Phys. Chem. B (submitted).
[25] B. E. Callicoatt, K. Forde, L. F. Jung, T. Ruchti, and K. C. Janda, J. Chem. Phys. **109**, 10195 (1998).
[26] J. Seong, K. C. Janda, N. Halberstadt, and F. Spiegelmann, J. Chem. Phys. **109**, 10873 (1998).
[27] K. P. Huber and G. Herzberg, *Molecular Spectra and Molecular Structure IV: Constants of Diatomic Molecules* (Van Nostrand Reinhold, New York, 1979).
[28] W. K. Lewis, R. J. Bemish, and R. E. Miller, J. Chem. Phys. **123**, 141103 (2005).
[29] K. von Haeften, T. Laarmann, H. Wabnitz, and T. Moller, J. Phys. B **38**, S373 (2005).
[30] K. von Haeften, A. R. B. de Castro, M. Joppien, L. Moussavizadeh, R. von Pietrowski, and T. Moller, Phys. Rev. Lett. **78**, 4371 (1997).
[31] K. von Haeften, T. Laarmann, H. Wabnitz, and T. Moller, Phys. Rev. Lett. **87**, 153403 (2001).
[32] K. von Haeften, T. Laarmann, H. Wabnitz, and T. Moller, Phys. Rev. Lett. **88**, 233401 (2002).